fire

MDPI

Article

Modal Analysis of a Fire-Damaged Masonry Vault

Armando La Scala [1,*], Pierpaolo Loprieno [2], Salvador Ivorra [3], Dora Foti [1] and Massimo La Scala [4,*]

[1] Dipartimento di Architettura Costruzione e Design, Polytechnic of Bari, 70125 Bari, Italy; dora.foti@poliba.it
[2] Dipartimento di Ingegneria dell'Innovazione, Università del Salento, 73100 Lecce, Italy; pierpaolo.loprieno@unisalento.it
[3] Departamento de Ingenieria Civil, Universidad de Alicante, San Vicente del Raspeig, 03080 Alicante, Spain; sivorra@ua.es
[4] Dipartimento di Ingegneria Elettrica e dell'Informazione, Polytechnic of Bari, 70125 Bari, Italy
* Correspondence: armando.lascala@poliba.it (A.L.S.); massimo.lascala@poliba.it (M.L.S.); Tel.: +39-329-317-3218 (M.L.S.)

Abstract: This study analyzes the thermo-mechanical behavior of a brick vault and the effect of a fire on its dynamic characteristics. Based on the results of an experimental test of a real barrel vault with a net span of 161 cm and a net rise of 46.5 cm, an accurate numerical model to simulate the behavior of the brick-and-mortar structure under thermo-mechanical stresses has been implemented. The comparison of the evolution of the displacement in the keystone and the temperatures at various points of the vault allows us to affirm that the adopted micro-modeling approach presents a good accuracy and a feasible computational effort. Finally, this study shows, from a numerical point of view, how the variation in the structure's eigenfrequencies can be predicted for extreme situations, such as fire damage. This aspect can be critical to develop effective intervention and prevention strategies, which can be useful for the preservation of our valuable cultural and historic resources.

Keywords: fire risk; masonry structures; modal analysis; thermo-mechanical behavior; numerical analysis

Citation: La Scala, A.; Loprieno, P.; Ivorra, S.; Foti, D.; La Scala, M. Modal Analysis of a Fire-Damaged Masonry Vault. *Fire* **2024**, *7*, 194. https://doi.org/10.3390/fire7060194

Academic Editor: Tiago Miguel Ferreira

Received: 17 April 2024
Revised: 30 May 2024
Accepted: 6 June 2024
Published: 8 June 2024

1. Introduction

From ancient buildings to contemporary infrastructure such as bridges and tunnels, masonry structures have been used for centuries in many different forms of construction. The complex characteristics of masonry buildings make it difficult to predict their response to load scenarios.

The problem of the thermo-mechanical response of masonry construction under fire situations is particularly relevant for existing buildings. Around the Mediterranean basin, and especially in Italy, masonry represents the most widespread building material, certainly the prevalent one for historical structures.

As an example, in Italy, a country with one of the most relevant historical/architectural heritages in Europe, out of more than twelve million residential buildings, about seven million are made of load-bearing masonry (ISTAT 2011 census [1]). These data can be combined with statistics on the number and type of interventions carried out by the fire brigades, according to which in 2021 about 30 percent of the calls received were related to fires and explosions; of this 30 percent, it can also be noted that about 15 percent were related to fires or explosions in apartments or living quarters, thus testifying to a certain vulnerability of the built environment to the phenomenon [2]. The problem of fire in masonry structures is a matter of structural integrity, and at the same time, of heritage preservation, as many of these buildings are an integral part of the historic fabric of the regions in which they are located. The challenge is compounded by

the dual need to protect life and preserve the architectural heritage encoded in these structures. The Italian government has shown serious interest in both prevention and preservation and conservation. In fact, Budget Law No. 145/2018 [3] approved the obligation to adapt the existing architectural heritage to the new Vertical Technical Rule (RTV) issued by the Ministerial Decree of 14 October 2021 [4], which thus completed the regulatory framework on fire prevention already initiated by the Cultural Heritage Code (issued by Legislative Decree No. 42/2004 [5]).

Regarding two-dimensional structural elements in masonry, a significant number of studies have been conducted with the objective of investigating the seismic response of such structures [6–14]. However, there are few studies that have investigated the response of such structures to significant thermal loads, such as those resulting from fires [15–17]. To the authors knowledge, no studies have been conducted to investigate the potential of modal analysis for assessing the structural health state of masonry vaults that have been affected by fire. This study is proposed as a preliminary approach to the subject matter.

A major problem for developing research in this direction is the difficulty of carrying out experimental tests and the associated safety issues.

A useful methodology in this regard is numerical modeling [17–20]. In fact, the construction of accurate finite element models (FEMs) makes it possible to simulate various stress conditions that may occur on a structure [21–24]. Finite element modeling has produced countless outstanding results over the years; therefore, regarding the case of masonry structures, we can distinguish three main approaches of constructing an FE model [25]:

- Detailed micro-modeling that distinguishes the different mechanical behavior of the brick (clay, stone or concrete) element from the mortar, reproducing the real geometry of both bricks and joints.
- Simplified micro-modeling, whereby the stone element is reproduced with increased dimensions that also consider the thickness of the mortar joints. Conversely, the mortar joints are considered only as interface surfaces.
- Macro-modeling, in which the masonry is considered as a homogeneous material without distinguishing between its different elements.

Detailed micro-modeling approaches have emerged [26–28] as a promising method for simulating the behavior of masonry structures. However, the computational cost of these approaches can be prohibitive for large structures or when detailed micro-scale characterization of the structure is not available.

To overcome these challenges, simplified micro-modeling approaches have been proposed to reduce the computational cost while still capturing the essential features of the structural behavior [29–33]. These approaches involve the modeling of the masonry structure as a set of interconnected blocks and the application of a simplified contact algorithm to simulate the interactions between two adjacent blocks. Despite their simplicity, these approaches have shown promising results in predicting the behavior of masonry structures under complex loading conditions [34].

In this paper, a simplified micro-modeling approach for predicting the thermo-mechanical behavior of masonry vaults is presented. A thermo-mechanical analysis to study the response of the masonry vault under various loading scenarios is performed and the simulation results are compared with experimental data. The predictive capability of the numerical approach is invaluable for understanding the vulnerability of existing structures and for designing new buildings that are more resilient to fire.

In the case where the simple stress and strain analysis is accompanied by modal analysis, it is possible to derive further insight into the structural integrity of masonry buildings when exposed to fire, as is already performed for earthquakes [35–38].

The objective is to propose an approach useful for the design and, in addition, a procedure to compare the state of the structure after a fire event with the ex ante state to preliminarily assess the safety of recovery operations and rehabilitation.

2. Basic Mathematical Formulation for Thermo-Mechanical Analysis

The focus of this study is investigating the vulnerability of a masonry vault to fire, a risk that is inherently related to the heat flux through the material and the specific fire load (q) and the resulting temperature gradients (T). These factors act as the physical agents of fire and require a thorough investigation to understand how the masonry vault will respond when subjected to such extreme conditions. The analysis splits into two distinct but interrelated paths—thermal and mechanical—both rooted in the fundamental properties of the materials, as shown in Figure 1. It is through a rigorous investigation that the overall resilience or vulnerability of the vault under fire conditions can be assessed.

Relevant for both thermal and mechanical analyses are the material properties of the vault. These properties include thermal conductivity (λ), density (ϱ), specific heat (c), coefficient of thermal expansion (α), and Young's modulus (E), which change with temperature. These intrinsic properties determine how the materials will interact with heat and withstand mechanical loads during a fire.

Thermal analysis examines how the vault absorbs and dissipates heat, changing its temperature profile. It examines the transient conditions that materials undergo when exposed to high temperatures. Meanwhile, mechanical analysis focuses on how heat affects the structural integrity of the vault. It looks at factors such as thermal expansion, which can cause stresses and deformations that can lead to structural failure and how material properties change with the temperature.

The results of these analyses converge in the global response of the vault, which is expressed in terms of stress (σ) and strain (ε). This global response encapsulates the overall behavior of the vault under fire conditions and provides insight into its stability and safety.

This allows researchers and engineers to predict how masonry vaults will respond to fire, with the goal of proving design and preservation strategies to enhance their resilience.

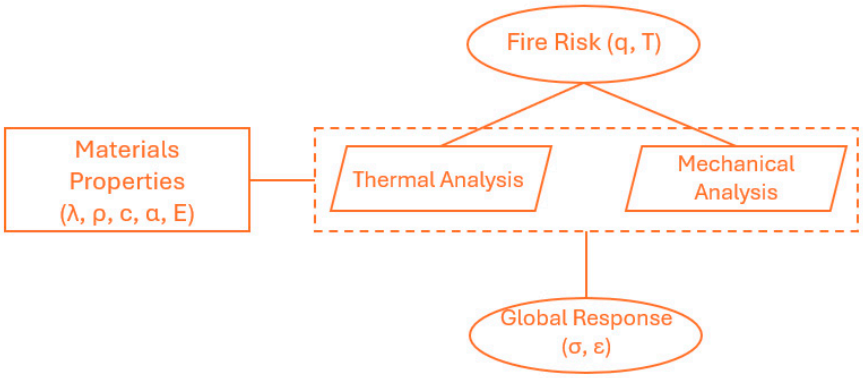

Figure 1. Schematization of the physical problem and its fundamental parameters.

2.1. Mechanical Equations

Many problems in computational mechanics are described by an approximate solution of variables such as displacements, deformations, stresses, forces, and possibly other state variables such as temperature within a solid subjected to some history of loading. "Loading" refers to a sequence of events whose response is being analyzed. Obtaining an accurate solution to such problems requires maintaining both force and moment equilibrium throughout any volume within the solid. The displacement finite element method simplifies this requirement by adopting a weaker form of equilibrium. Instead of requiring exact equilibrium, it ensures that equilibrium is achieved on average over a finite number of subdivisions of the solid volume. The basis for developing a displacement–interpolation finite element model is to create a local spatial approximation

for portions of the solution. This process begins by transforming the equilibrium equations into a "weak form"—a single scalar equation that spans the entire body. This is achieved by multiplying the point-wise differential equations by an arbitrary, vector-valued "test function", which is defined conveniently continuously over the entire volume, and integrating the result [39]. Due to the arbitrary nature of the test function, the differential equilibrium in any given direction at any given point can be precisely determined by choosing the test function to be nonzero only in that direction at that point. In scenarios where equilibrium is considered with a general stress matrix, this "weak form" corresponds to the virtual work principle. The test function is conceptualized as a "virtual" velocity field that is arbitrary but has to obey some kinematic constraints and has a sufficient continuity. The interaction of this test function with the equilibrium force field then represents the rate of "virtual" work performed. The complete form of the virtual works theorem is reported as follows in Equation (1):

$$\int_V \boldsymbol{\sigma} : \delta \boldsymbol{D}\, dV = \int_S \delta \boldsymbol{v} \cdot \boldsymbol{t}\, dS + \int_V \delta \boldsymbol{v} \cdot \boldsymbol{f}\, dV \quad (1)$$

where σ is the Cauchy stress matrix for each point of the surface S; $\delta \boldsymbol{D}$ is the antisymmetric part of the virtual velocity gradient, also known as virtual strain rate; $\delta \boldsymbol{v}$ is the arbitrary test function, imagined as a "virtual" velocity field; $\boldsymbol{t}$ is the traction vector per unit area in S; $\boldsymbol{f}$ is the force vector for volume unit; V denotes a volume occupied by a part of the body in the current configuration; and S is the surface bounding V.

The virtual work principle offers a simple physical interpretation: the rate of work performed by external forces under any given virtual velocity field is equal to the rate of work performed by stress forces counteracting the deformation rate within the same virtual field. This principle serves as the "weak form" of the equilibrium equations and forms the basic equilibrium relation for finite element analysis. Its usefulness lies in the fact that it represents equilibrium as an integral over the volume of the body and allows for the incorporation of approximations through the selection of test functions for the virtual velocity field. These test functions are not completely arbitrary; their variation is restricted to a finite set of node values. This method provides a more robust mathematical framework for investigating approximations than the direct discretization of derivatives found in the differential equilibrium equations that typically underlay finite difference methods for addressing similar problems.

2.2. Thermal Equations

From the thermal point of view, the equation adopted to evaluate the heat transfer is Fourier's law, expressed as in Equation (2):

$$\boldsymbol{f} = -\boldsymbol{k}\frac{\partial \theta}{\partial \boldsymbol{x}} \quad (2)$$

where $\boldsymbol{k}$ is the conductivity matrix, **f** is the heat flux, θ is the temperature, and **x** the position vector. Conductivity **k** can be anisotropic, orthotropic, or isotropic.

The boundary conditions can be expressed as a fixed temperature, a fixed heat flow through a surface, a fixed heat flow through a volume, surface convection, and radiation.

2.3. Thermo-Mechanical Coupling

The numerical simulation has been performed adopting a well-known solver, Abaqus/Explicit. In the explicit heat transfer analysis, the heat transfer equations are integrated using the explicit forward difference time integration rule. The temperature at node *N*, denoted by θ^N, is updated at each increment, denoted by the subscript i according to this rule. The forward difference integration is such that it does not require the simultaneous solution of equations because it uses a lumped capacitance matrix. The current temperatures are calculated using the known temperatures obtained from the previous increment.

The updated temperature is given by Equation (3):

$$\theta_{(i+1)}^{N} = \theta_{(i)}^{N} + \Delta t_{(i+1)} \dot{\theta}_{(i)}^{N} \quad (3)$$

and the rate of temperature change as reported in Eq. (4):

$$\dot{\theta}_{(i)}^{N} = (C^{NJ})^{-1}\left(P_{(i)}^{J} - F_{(i)}^{J}\right) \quad (4)$$

where C^{NJ} represents the lumped capacitance matrix, P^{J} is the applied nodal source vector, and F^{J} is the internal flux vector.

In Abaqus/Explicit, the explicit dynamics simulation is based on the implementation of an explicit integration rule, together with the use of diagonal ("lumped") element mass matrices. The equations of motion for the body are integrated using the explicit central-difference integration rule represented by Equations (5) and (6):

$$\dot{u}_{\left(i+\frac{1}{2}\right)}^{N} = \dot{u}_{\left(i-\frac{1}{2}\right)}^{N} + \frac{\Delta t_{(i+1)} + \Delta t_{(i)}}{2} \ddot{u}_{(i)}^{N} \quad (5)$$

$$u_{(i+1)}^{N} = u_{(i)}^{N} + \Delta t_{(i+1)} \dot{u}_{\left(i+\frac{1}{2}\right)}^{N} \quad (6)$$

Here, u^{N} represents a degree of freedom (a displacement or rotation component) and the subscript i denotes the increment number in an explicit dynamics step. The central-difference integration operator is explicit in the sense that the kinematic state is advanced using known values of $\dot{u}_{\left(i-\frac{1}{2}\right)}^{N}$ and $\ddot{u}_{(i)}^{N}$ from the previous increment. The key to enhance the computational efficiency in this solver is the use of diagonal element mass matrices, as the accelerations are calculated when evaluating the increment as follows in Equation (7):

$$\ddot{u}_{(i)}^{N} = (M^{NJ})^{-1}\left(P_{(i)}^{J} - I_{(i)}^{J}\right) \quad (7)$$

where M^{NJ} is the mass matrix, P^{J} is the applied load vector, and I^{J} is the internal force vector. The mass matrix is "lumped" to simplify its inverse computation and because the vector multiplication of the mass inverse by the inertial force requires only n operations, where n is the number of degrees of freedom in the model. The explicit procedure requires no iterations and no tangent stiffness matrix. The internal force vector, I^{J}, is assembled from the contributions of each element, eliminating the need to form a global stiffness matrix.

In an explicit integration scheme, it is necessary to have nodal mass or inertia at all activated degrees of freedom. Specifically, non-zero node mass should be assumed unless all activated translational degrees of freedom are constrained, and non-zero rotational inertia is required unless all activated rotational degrees of freedom are similarly constrained. Nodes that are integral to a rigid body structure do not require mass individually, but the rigid body must have a specified mass and inertia.

Nodal mass or inertia comes into play when nodes are activated by elements with non-zero mass density, such as those found in solid, shell, or beam structures, or by mass and inertia elements themselves. The accumulation of lumped mass contributions occurs naturally from these elements.

Conversely, when nodes are activated by massless elements such as springs, dashpots, or connectors, care must be taken. One must either constrain the node or add mass and inertia in a way that makes physical sense and is consistent with the dynamics of the system.

The response of the mechanical system is determined using the explicit "central-difference integration rule" with a lumped mass matrix. The heat transfer and mechanical responses are calculated simultaneously through explicit coupling, eliminating the need for iterative solutions or tangent stiffness matrices.

This explicit integration approach is generally more computationally efficient and streamlines the handling of contact conditions between elements.

The stability of the explicit integration process is guaranteed for small time steps depending on conditionally stable central-difference and forward-difference operators. The stability limit, which does not consider any damping effects in the mechanical solution, can be determined by the following criterion reported in Equation (8):

$$\Delta t \leq \min\left(\frac{2}{\omega_{\max}}, \frac{2}{\lambda_{\max}}\right) \tag{8}$$

In this context, $\omega_{\max}$ is the highest angular frequency in the equation set of the mechanical system, and $\lambda_{\max}$ is the largest eigenvalue in the equation set of the thermal system. This stability criterion ensures that the time step is sufficiently small to capture the dynamics of the system without introducing numerical instability [39].

3. Masonry Vault Modeling

To accurately represent the thermo-mechanical behavior of a masonry structure in a numerical environment, a complete knowledge of the microscale characteristics of the structure, including the geometry and orientation of individual brick and mortar joints, is required [40]. Thus, the development of a numerical model sufficiently accurate for masonry structures should consider:

- The materials (through simplified or complex constitutive relationships);
- The masonry element;
- The nonlinearity, both at the material level and at the geometric element level;
- The construction details and their effect on the masonry walls (e.g., the presence of curbs, infinitely rigid or deformable soils, or those characterized by their real stiffness, degree of wall buckling, etc.).

Therefore, our work is placed within this line of research, with the further aim of providing useful indications for the analysis and study of some buildings of historical/architectural value.

The modeling procedure applied to a masonry structure is influenced by the level of detail adopted, both in terms of materials and structural elements. It is also necessary to consider the type of analysis to be undertaken, the results of which, as well as the computation time, will be influenced by the level of detail chosen.

When the performed analysis is nonlinear, it is also necessary to choose how to model the nonlinearity of the inelastic behavior of the element: in these cases, the macro distinction concerns concentrated or distributed plasticity models.

FE Modeling

To define a simplified micro-model, the vault has been represented by three-dimensional solid elements with average mechanical and thermal properties of the clay bricks and the mortar. All blocks were modeled with increased dimensions to consider the thickness of the mortar courses, i.e., the numerical block is an "equivalent block" that is realized considering the real dimensions of the block and half of the thickness of the mortar joints on each side [25]. On the other hand, the mortar behavior is defined by the mutual interactions between the blocks in both main directions to obtain a realistic representation of the overall behavior [41–43]. Given the limitations imposed by the computational machine used, to reduce the computational burden of the test, it was decided to define a model with a smaller size that considered the vault in its elevation between the shuttering sections, but with a reduced longitudinal section, made by one brick and half, which is equally significant for the global behavior of the structure. This was possible because the characteristics of the vault were constant throughout its entire longitudinal development.

The blocks are modeled using C3D8T elements (ideal for coupled temperature–displacement analyses) with a total of 42,000 elements and 61,600 nodes. Such a high number of elements was used because the ultimate purpose of our analyses goes beyond evaluating displacements and aims to include the influence of temperature on structural behavior. The elements comprising the model are defined as deformable elements with associated nonlinearity and cracking characteristics. The blocks were modeled according to an elasto-plastic type of constitutive bond, in which the plastic phase is described by a particular extension of the Drucker–Prager criterion.

The nonlinear characteristics of the structure were simulated using the plasticity model known as Concrete Damage Plasticity (CDP). CDP is a material nonlinearity model generally used for brittle materials subject to static and dynamic loads and based on the theory of plasticity and damage mechanisms [44–47]. Essentially, this model is a development of the Drucker–Prager model, modified by a coefficient K_c to define a difference between compressive and tensile yield stresses and a coefficient expressing the ratio of biaxial to uniaxial compressive yield stresses.

The failure is governed by a criterion known as "Quadratic Nominal Stress Damage" (Quads Damage in Abaqus), which evaluates the stress ratios between a given stress value and the peak nominal stress value in each of three directions [39].

To simulate heat transfer inside the vault, conductivity and specific heat parameters obtained as average parameters between data from data sheets of similar materials were set for the blocks. To better simulate the influence of temperatures on the structural behavior of the vault under consideration, an important feature of the proposed approach is that the parameters entered for the definition of materials vary in relation to temperatures. The parameters were identified from the literature and selected for similarity to the case under consideration. Data that could not be identified in the literature were instead assessed through a parametric study. The data set needed to calibrate the model are shown in Tables 1–4.

Table 1. Elastic properties of equivalent brick in Abaqus.

Elastic Properties of Bricks			
Density	kg/m^3	1721	Experimental data [48]
Young's modulus	MPa	1100	Norme Tecniche per le Costruzioni (NTC 2018) [49]
Poisson's Coefficient	-	0.25	Norme Tecniche per le Costruzioni (NTC 2018) [49]

Table 2. Concrete Damage Plasticity properties of an equivalent brick in Abaqus.

Post-Elastic Properties of Bricks			
Dilatancy angle		10	Naciri et al. 2022 [50,51]
Eccentricity	-	0	0–0.1 from Drucker-Prager Theory [44,52,53]
f/f_{b0c0}	-	1.61	Naciri et al. 2022 [50,51]
K	-	0.667	Naciri et al. 2022 [50,51]
Viscosity	-	0.002	For Abaqus convergence [54]
Compression strength	MPa	2.89	Norme Tecniche per le Costruzioni (NTC 2018) [49]

Table 3. Quads damage properties of an equivalent brick in Abaqus.

Quads Damage and Damage Evolution Parameters of Bricks			
Nominal Stress Normal-Only mode	N/mm²	0.04	Ptaszkowska et al. 2014 [55]
Nominal Stress First Direction	N/mm²	0.056	1.4*Normal stress (Abdulla et al. 2017) [56]
Nominal Stress Second Direction	N/mm²	0.056	
Normal Mode Fracture Energy	N/mm	0.02	Ptaszkowska et al. 2014 [55]
Shear Mode Fracture Energy First Direction	N/mm	0.125	Abdulla et al. 2017 [56]
Shear Mode Fracture Energy Second Direction	N/mm	0.125	

Table 4. Thermal properties of equivalent brick in Abaqus.

Thermal Properties of Clay Bricks			
Conductivity	W/mK	1.092	Norme Tecniche per le Costruzioni (NTC 2018) [49]
Specific heat	J/kg °C	922	

Regarding the interactions between the blocks, the goal is to reproduce the mechanical behavior of the mortar. Therefore, it is necessary to define both tangential and normal behavior, as well as mechanical capabilities. In the normal direction behavior, the hard contact option was used, which defines the impossibility of interpenetration between the blocks. For tangential behavior, the "penalty" option [39] was used, with which the friction limit angle and shear stress limit are associated. For the definition of mechanical parameters, the cohesive properties and damage limit state were defined using the cohesive and damage options. The cohesive assumption handles the linear behavior through an elastic stiffness matrix that characterizes the linear tensile separation relationship. Damage handles the post-elastic response that is characterized by crack propagation and is defined by the maximum nominal stresses in the normal and shear components that govern the onset of the cracking phase, the cracking energies (again in the normal and shear components, according to Benzeggagh–Kenane behavior), and finally by crack stabilization governed by a viscosity coefficient. The thermal characteristics of the mortar were associated with the interactions to simulate the thermal transmission capabilities of the mortar. The characteristics of the interface bond in the numerical model are shown in Table 5.

Table 5. Interaction properties at the interface between the equivalent bricks in Abaqus.

Interaction Properties at the Interface between Bricks			
Friction Coefficient	-	0.43	
K_{nn}	N/mm³	21	
K_{ss}	N/mm³	8.4	
K_{tt}	N/mm³	8.4	
Maximum Normal Nominal Stress	N/mm²	0.04	Ptaszkowska et al. 2014 [55]
Maximum Normal Shear Stress	N/mm²	0.173	
Normal Fracture Energy	N/mm	0.173	
First Shear Fracture Energy	N/mm	0.02	
Second Shear Fracture Energy	N/mm	0.05	
Viscosity Coefficient	-	0.002	For Abaqus Convergence [54]

For the definition of a coupled displacement and temperature analysis, it is necessary to define the boundary conditions. The vault was hinged to the support section, and the presence of the blocking elements on the front and back of the vault was modeled by

imposing restrictions on lateral displacements and out-of-plane rotations on both mentioned faces.

The analysis chosen to simulate the test is explicit dynamic coupled temperature–displacement analysis, as defined in Abaqus, which allows the good performance of the analysis to be verified through the kinetic energy and total energy values provided step by step.

4. Thermo-Mechanical Analysis

To verify the suitability of the adopted assumptions for the numerical model, the temperatures and displacements obtained from an experimental test, conducted at the Roma-Capannelle Fire Department Experimental Center [48], were compared with those obtained from our simulation in Abaqus.

4.1. Experimental Campaign

The masonry vault was built in a horizontal furnace under simple support conditions on two HEB 200 section steel girders. The vault has a net span of 161 cm and a rise of 46.5 cm. The length of the intrados arch measures 195 cm. The thickness of the vault is 12 cm. The bricks specific weight is estimated to be 1800 kg/m^3 (NTC 2018 tab. 3.1.I) [49].

The load is applied by two concentrated forces symmetrically distributed in the longitudinal direction of the vault at about 50 cm from the axis. The quantification of the load to be applied is performed by applying the static theorem of limit analysis. The arrangement of the funicular polygon ensures verification of external equilibrium compatibility.

The load multiplier is increased until the condition of tangency of the funicular polygon with the central inertia core of the masonry section is reached. Following that, a load of 9.2 kN was applied to the vault. The geometric dimensions of the vault are reported in Figure 2.

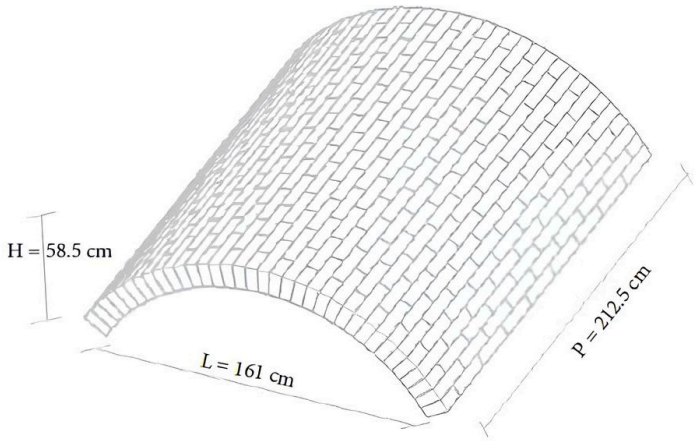

Figure 2. Experimental vault as built in the laboratory of Roma-Capannelle.

The simplified method in Appendix C of Eurocode EN 1996-1-2 is adopted for fire resistance time calculation [57], supplemented by DCPREV circular 4638 [58]. In this method, the resistant section is reduced according to the values of the maximum temperature reached in the section. For masonry made of artificial elements and mortar, the European standard provides the limiting temperature values shown in Table 6:

Table 6. Temperature limit values for thermal tests on masonry in Eurocode [57].

Unprotected Bricks and Mortar	Constant c	Temperature [°C]	
		θ_2	θ_1
Clay bricks with generic mortar	c_{cl}	600	100
Calcium–silicate bricks with a thin layer of mortar	c_{cs}	500	100
Lightened blocks with pumice and generic mortar	c_{la}	400	100
Heavy bricks with generic mortar	c_{da}	500	100
Autoclaved aerated blocks with thin mortar layer	c_{aac}	700	200

Below 100 °C, the material can be considered fully resistant, above 600 °C it offers no mechanical strength, and between 100 °C and 600 °C the material has an intermediate strength, which, since it is not specified by the Eurocode or its National Annexes [57–59], can be cautiously set to zero by virtue of DCPREV Circular 4638 [58].

The vault was then heated following a temperature gradient that traced the temperature curve prescribed by ISO Standard 834 for fire tests on structures [60].

Experimental verification of the vault exposed to fire is carried out by evaluating:

- The bearing capacity R, by measuring subsidence and the rate of subsidence;
- Thermal insulation, by placing thermocouples on the unexposed face.

The test was conducted for 55 min, sufficient to study the behavior of the structure beyond the maximum calculated fire resistance time (45 min).

4.2. Deviations in Numerical Method

In the numerical model, several deviations from the experimental test system have been made. As for the application of load, it was applied as pressure on the extrados of the vault and imposed as a total load, circumventing the direct modeling of the concrete curb, wooden board, and steel plate, which were instead used in the experimental test to ensure uniformity of load distribution. About the constraint conditions, hinges were modeled at the support nodes of the structure, as shown in Figure 2. This is due to the fact that during the experimental phase, the vault was never in a real interlocking condition, as was also confirmed to us by the fire brigade officials during discussions with them. The assembly of the structure in the FE Model is shown in Figure 3.

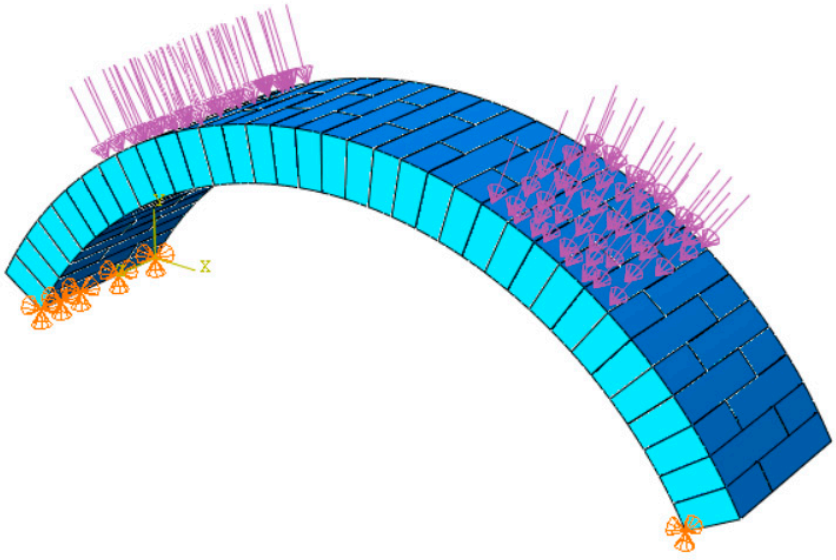

Figure 3. Reconstruction of the vault in Abaqus.

The thermal load is defined by a field in which the imposed field simulates the furnace condition, a temperature rise according to the ISO 834 curve [60]. Since the temperature in the experimental test is imprinted precisely by an increase in temperature in the furnace and not by a thermal load applied directly to the vault, it was necessary to define boundary conditions that simulated the presence of air, or rather its convection and radiation capabilities. This condition was simulated by defining a convection and radiation film at the intrados. In this way, the convection and radiation characteristics of the air are defined by associating them with the thin transition section between the air and the vault. For this purpose, both convection and radiation coefficients that regulate the thermal flow in the fluid has been defined in the model. At the extrados, the same parameters need to be defined to simulate the heat flow exchange between the masonry vaults and the ambient air.

4.3. Model Validation

A calibration process to tune the parameters of the numerical model which represent the effect of the interface between blocks is needed. In fact, the calibration allows us to fit the numerical results with measurements obtained on the experimental test. The calibration process involved both mechanical and thermal parameters of the interface properties between the blocks.

Regarding the mechanical parameters, the trend of the deflection in the keystone was compared, whereby it was verified that the keystone section underwent the same lowering as the vault did during the experimental tests. As for thermal parameters, three points were identified in the model, at the intrados, extrados, and in the middle section at the keystone section, against which the temperature trend was evaluated and compared with that measured by thermocouples at the same positions during the experimental campaign (T2, T8, T29). These points have been chosen because they correspond to the highest temperatures measured at the intrados of the vault and on the inside. The positions on the vault are reported in Figure 4. The computational load of the test is 7100 s.

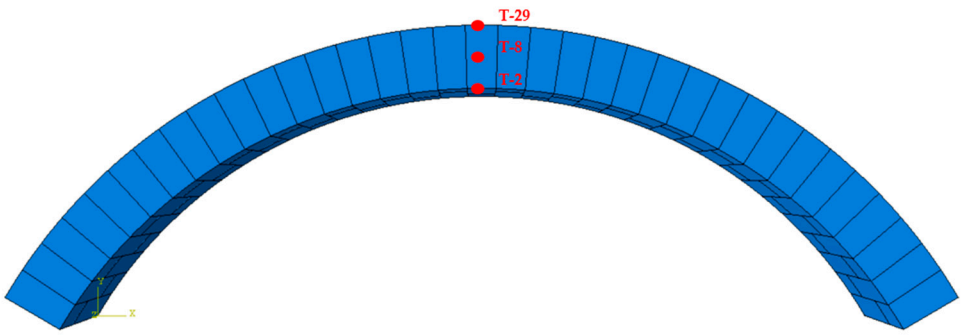

Figure 4. Thermocouples positions.

Comparing the results obtained by the numerical model with those obtained by the experimental test, a good match with the physical model can be observed. In fact, by analyzing the tensional state, the fracture mechanism is evident, showing the formation of three hinges, two lateral and one at the keystone section. Upon reaching the plastic phase at those points, crack formation is confirmed, as occurred in the experimental phase.

This is also confirmed by comparing the displacements of the key section of the numerical model with those of the experimental campaign, which have a relative error of 2% that we consider highly acceptable. In contrast, the difference between the displacements of the sections below the point of load application is larger. This discrepancy results from the simplification of the model regarding how the load is applied. In the experimental phase, the reading of the subsidence of the section below is

taken by the machine itself applying the load. This means that the read subsidence is that of the vault plus the deformation of the concrete, wood, and steel elements that distribute the load uniformly over the entire vault. The displacement measures are presented in Table 7.

Table 7. Displacement correspondence between experimental results and numerical test.

	Displacements at the Control Points at Min 52		
	Experimental (mm)	**Numerical (mm)**	**Error (%)**
Keystone	4.46	4.36	1.13
Load line	12.83	9	17.54

Analyzing the thermal behavior, the temperature trends at selected control points are shown in Figures 4–6. A good correspondence between the numerical and experimental curves emerges. As for the curve of the central point, it is mainly influenced by the thermal characteristics of the vault itself since heat exchange occurs by conduction. Due to this, the application of the same heating curve as the experimental one resulted in a very accurate match between the real case and the numerical test, as shown in Figure 5.

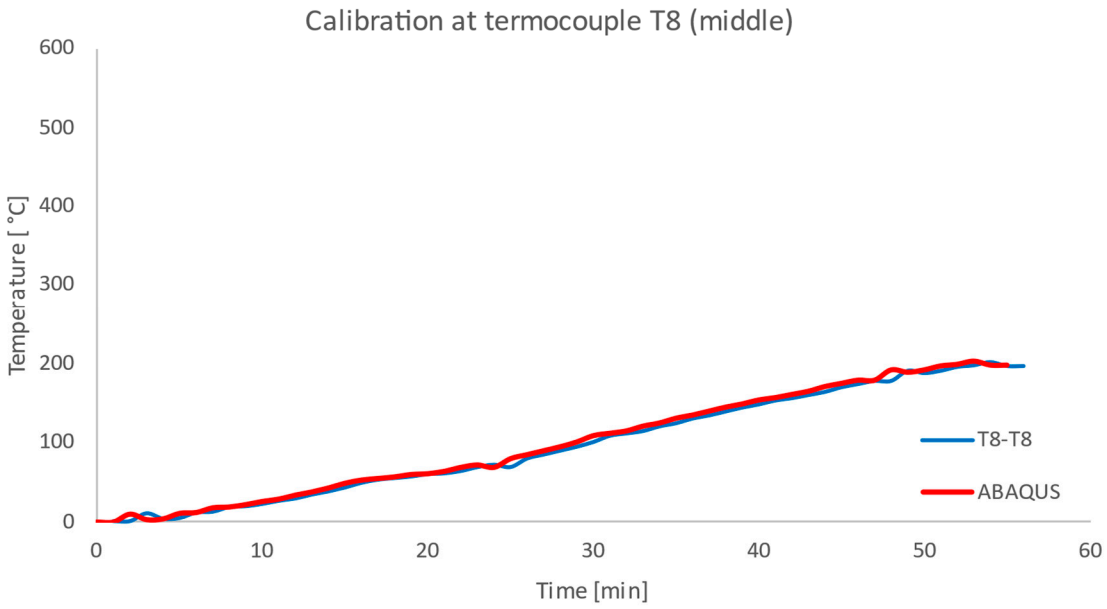

Figure 5. Temperatures calibration in the middle of the vault section at 5 cm from the intrados.

For points at the intrados and extrados of the vault, the matter is different. At these points, the temperatures depend mainly on the interactions and thermal exchanges between the air and the vault, and thus both radiation and convection phenomena are involved. Temperatures at the intrados show a very good correspondence with those obtained in the experiment, as can be seen in Figure 6.

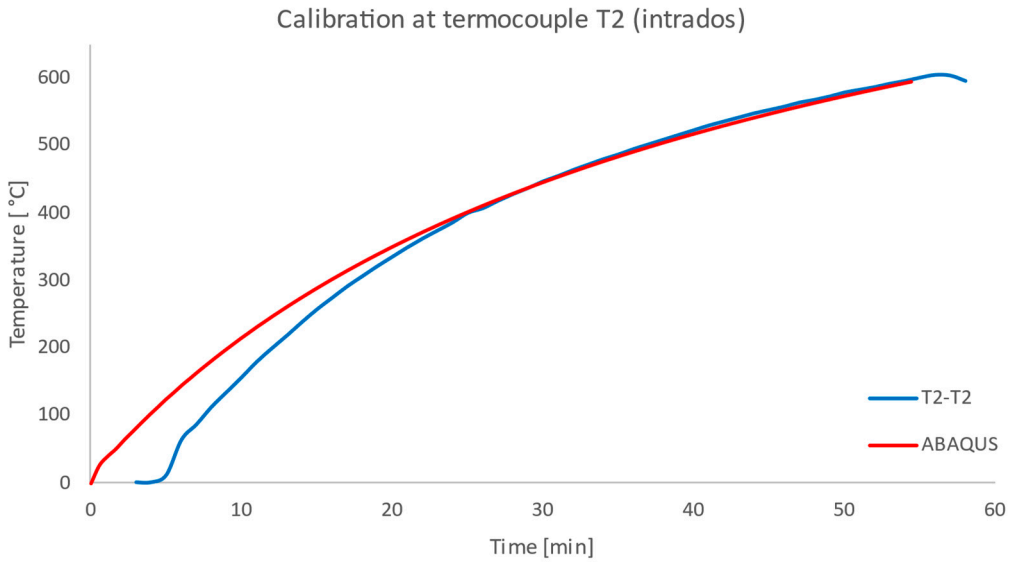

Figure 6. Temperature calibration at the intrados of the vault.

At the extrados, due to the computational burden, we chose not to define the heating loss conditions in the numerical model, but the results show an acceptable difference, as can be seen in Figure 7.

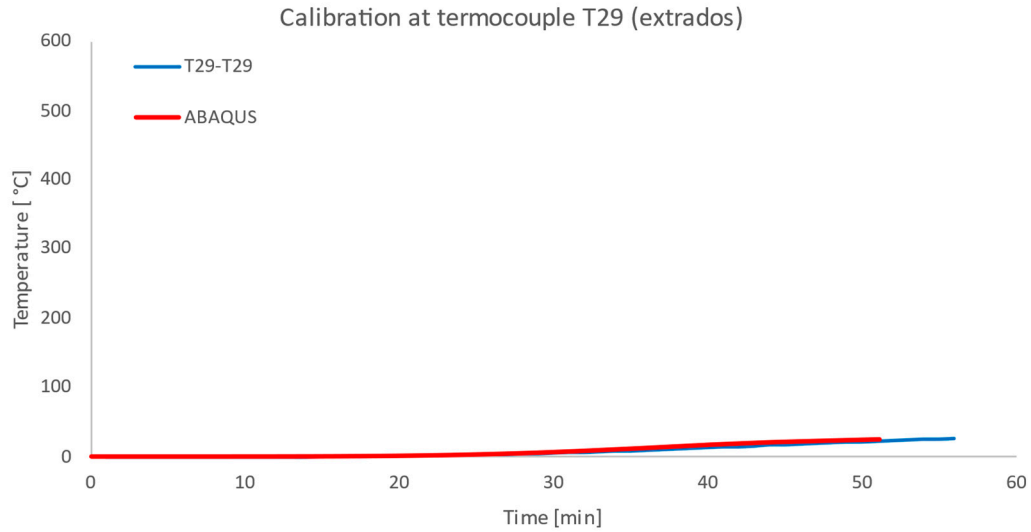

Figure 7. Temperature calibration at the extrados of the vault.

Another relevant aspect that has been observed in the numerical environment is the accurate reproduction of the crack pattern in the parts of the structure not influenced by the constraint conditions. The proposed FE model allows us to evaluate the crack formation through the damage level of all the nodal joints. The damage is defined through CSMAXCRT, which is the value of maximum traction damage for cohesive interactions, which have been used to represent the binding properties of mortar joints. This makes it possible to use it to predict the damage evolution of the vault under different loading conditions. Through Figures 8 and 9, it is possible to compare what is observed in the experimental test and in the FE model.

Figure 8. Crack pattern (red dot line) at the keystone in the experimental test.

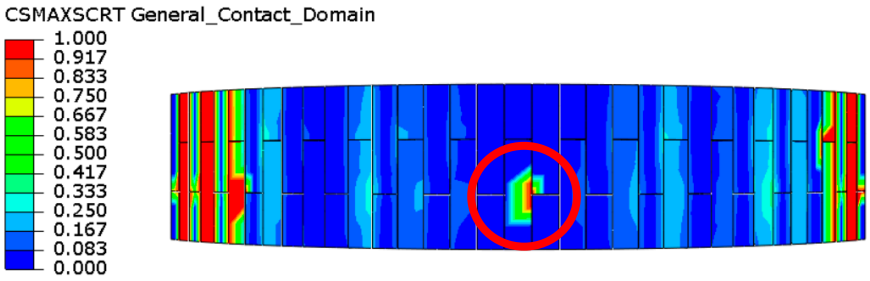

Figure 9. Crack pattern at the keystone in the FE model.

5. Modal Analysis

Modal analysis (MA) proved to be an important technology for the study of structural dynamics. Through modal analysis, complex phenomena in structural dynamics can be represented using decoupled modes consisting of natural frequency, damping, and mode shapes. The collection of these modal parameters is called a Modal Model.

Comprehensive modal analysis includes both data acquisition and subsequent parameter identification. From its inception to the present, modal analysis has been widely applied in mechanical and structural engineering for design, optimization, and validation purposes. It has been widely accepted for broad applications in automotive, civil engineering, aerospace, power generation, musical instruments, etc.

The key features of a Modal Model are natural frequency, damping, and mode shapes. The natural frequency is the frequency at which a structure vibrates in the absence of external forcing; this identifies the resonance conditions that can cause the structure to fail. Damping describes the loss of energy during the vibration of the structure and tends to have a stabilizing effect on the structure. The mode shapes describe the pattern of displacement a structure goes through at each natural frequency, helping to predict stress concentration and the possibility of failure [61].

5.1. Theoretical Framework

Modal analysis is a technique for describing the dynamic behavior of mechanical systems. It employs experimental methods that focus on the exploration of modal shapes. It typically involves the mechanical excitation of a structure using instruments such as hammers or shakers, while the vibration data are collected by an array of sensors, primarily accelerometers. In the field of structural analysis, modal analysis is instrumental in elucidating both the inherent properties and the dynamic responses of structures, regardless of their state of constraint. It adeptly addresses scenarios where the structure operates in isolation or is subject to externally applied dynamic forces, providing a comprehensive understanding of its dynamic performance.

Analytically, modal analysis consists of solving an eigenvalue problem associated with the equation of motion, Equation (9):

$$\mathbf{M}\{\ddot{\boldsymbol{u}}(\mathrm{t})\} + \mathbf{C}\{\dot{\boldsymbol{u}}(t)\} + \mathbf{K}\{\boldsymbol{u}(t)\} = \{\boldsymbol{f}(t)\} \quad (9)$$

where **M** is the mass matrix, **C** is the matrix of damping coefficients, **K** is the stiffnesses matrix, **u**(t) is the displacement vector and its derivatives, **f**(t) is the generic force vector.

In the case of structures that have been subjected to fire or other particularly destructive phenomena such as earthquakes, forced excitation of oscillation modes is not possible, so operational modal analysis (OMA) is often used [62,63]. These methodologies focus on determining the modal characteristics of structures by analyzing only their vibration responses. Typically, this analysis is conducted under normal operational conditions; i.e., under environmental vibrations, OMA offers the advantage of minimal disruption to a structure's everyday usage and is cost-effective. Additionally, the modal properties derived from OMA reflect the true operational behavior of the structure. Data analysis for OMA can be performed in either the time or frequency domain. The obtained modal information is crucial for evaluating the structure's response to dynamic forces and, in certain cases, can also be instrumental in assessing structural health and performance.

Usually, the results of operational modal analysis are used for model updating, i.e., for calibration of numerical models that have some inaccuracies due to the obvious simplifications assumed in the numerical field. In some cases, however, it is also possible to reverse the procedure, i.e., to use appropriately calibrated numerical models to preliminarily study the behavior of a structure under critical conditions and to use the results to guide field interventions when the catastrophic event occurs.

5.2. Numerical Frequencies

Frequency calculation is developed by the Abaqus 2017/CAE solver through the resolution of an eigenvalue problem. By extracting the eigenvalues, the software allows calculation of the natural frequencies and corresponding modal forms of a system. The calculation also considers initial stress states and the effects induced on stiffness by previous load states. In addition, the procedure can calculate residual modes if necessary. It is important to note that this is a linear perturbation procedure. A significant advantage of this methodology is the ability to perform the calculation in parallel on multiple CPUs [39].

The eigenvalue problem for the natural frequencies of an undamped finite element model is represented by the Equation (10):

$$(-\omega^2\mathbf{M} + \mathbf{K})\{\boldsymbol{\phi}\} = 0 \quad (10)$$

where:

- **M** is the mass matrix, with M×N degrees of freedom, and is symmetrical and positively defined;
- **K** is the stiffness matrix, with M×N degrees of freedom. It includes the effects of the initial stiffness if the starting state included any geometric nonlinearities;
- **ϕ** is the eigenvector of dimension N (the mode of vibration);

When **K** is positively defined, all eigenvalues are real and positive. Rigid body motions make the value of the stiffness tensor undefined, returning zero eigenvalues; conversely, instability phenomena induce negative eigenvalues. The adopted resolution method is the "subspace iteration method". With this method, having defined the required number of eigenvalues, the Abaqus/CAE solver chooses an appropriate number of vectors for iteration, after which it extracts eigenvalues until the required number of eigenvalues is reached or the last calculated frequency exceeds the maximum frequency of interest.

Analyses were performed both on the vault in the undisturbed state, with only the presence of the backfill loads and on the vault at the end of the fire simulation. The numerically derived frequency values are presented in Table 8.

Table 8. Frequencies and periods obtained by the numerical model for the undamaged vault and for the fire-damaged vault.

	Ex Ante		Ex Post		Difference (%)	
	Frequencies [Hz]	**Periods [s]**	**Frequencies [Hz]**	**Periods [s]**	**Frequencies**	**Periods**
1	51.96	0.019246	46.29	0.021603	−10.91	12.25
2	86.28	0.01159	79.71	0.012545	−7.61	8.24
3	116.76	0.008565	105.45	0.009483	−9.69	10.73
4	135.38	0.007387	124.74	0.008017	−7.86	8.53
5	137.42	0.007277	128.78	0.007765	−6.29	6.71

Eigenfrequencies decrease after the fire by a factor between 10 and 6 percent. In Figure 10 a comparison between ex ante (before fire) and ex post (after fire) frequencies is presented in a diagram form.

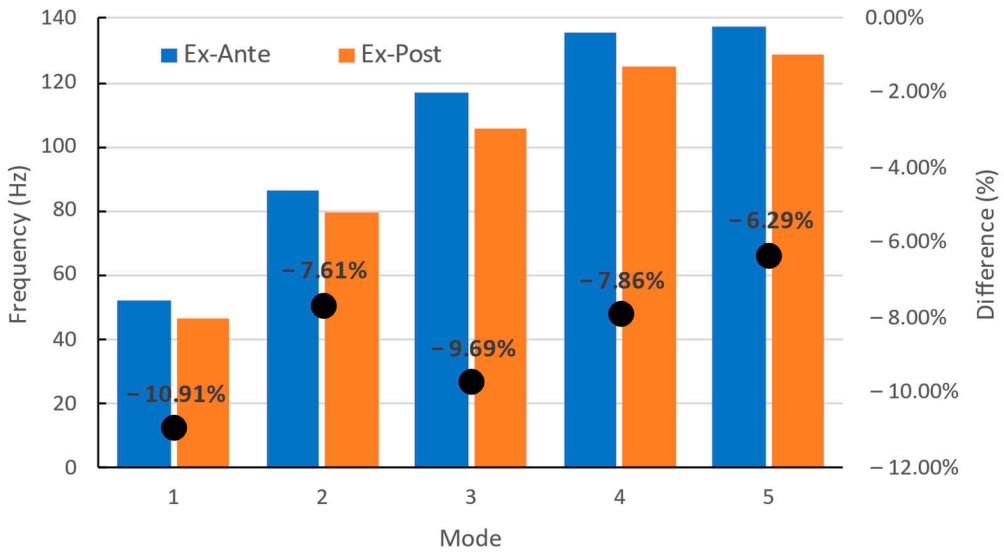

Figure 10. Comparison of pre- and post-damage frequencies corresponding to each main mode.

The health state of a structure can be monitored during time through modal analysis as can be proved in previous works [36,64–70].

The numerical analysis reported in Figure 10 shows how the frequencies compared before and after the fire provide a useful measure of the degree of damage to the structure. This observation can lead to the definition of a practical method to assess the structural safety by applying a set of accelerometers to measure frequencies based on the environmental vibrations. If a numerical model is built with a reasonable degree of accuracy, the frequency decays, observed in the numerical simulation in correspondence with a major damage of the structure, can be compared with actual frequency measurements to assess the degree of the damage to the physical structure after a fire; i.e., the numerical model is used as a digital twin of the physical structure.

A further analysis was performed to understand how the stiffness of the structure degrades with the temperature of the fire.

Frequency decay with temperature was evaluated since this quantity is directly correlated to the stiffness of a structure, at least in the elastic field. Being able to define a

nonlinear correlation between the frequency and stiffness of the masonry would be extremely useful as it would allow us to define an index of the decay of the mechanical parameters of the constituent materials and not just a definition of the degree of risk

The trend of the frequency decay for the first mode as temperature increases is shown in Figure 11. This mode was selected for brevity since it is the one which experienced the largest reduction. The function approximated by interpolation follows a power law with negative exponent.

This behavior shows how even fires characterized by a moderate increase in the temperature can give rise to a significant decay in the stiffness properties of the structure. Consequently, frequency measurements on the actual structure can provide an insight into the damage caused by a fire when compared with a digital model and assess the temperatures reached during the fire. This decay of frequencies with the fire temperature tends to saturate for high temperatures, meaning that when numerous cracks in the structure appear, the stiffness and the structural safety of the vault are irremediably lost.

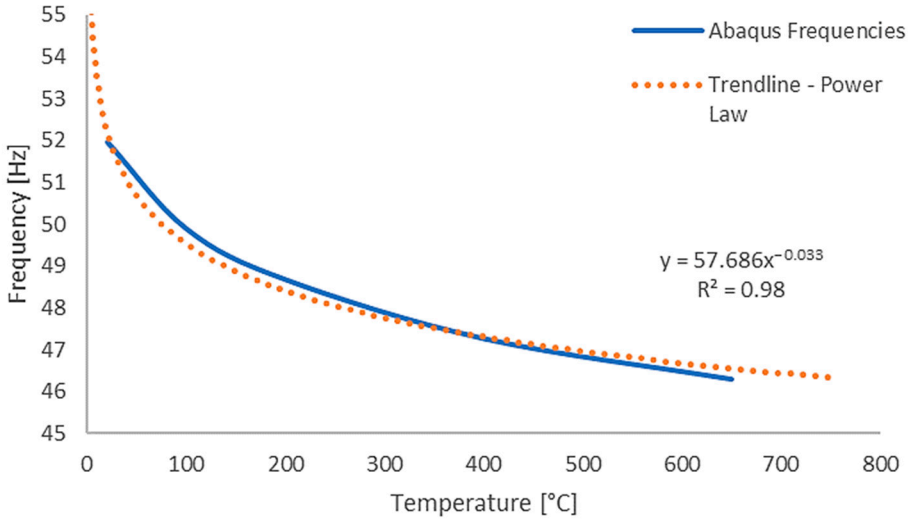

Figure 11. Decay of frequencies at the first mode as function of temperature.

6. Conclusions

This work investigates the possibility of using modal analysis and numerical models to determine the health status of a structure after being exposed to fire.

For this purpose, a numerical finite element model is built in Abaqus/CAE to replicate the thermo-mechanical behavior of a masonry vault by modeling the structure through equivalent blocks connected by cohesive properties that simulate the presence of the mortar joints.

This work has produced several outcomes:

1. A simplified micro-model in which a thermo-mechanical analysis has been conducted, in good agreement with experimental tests in terms of measured temperatures and displacements.
2. The FE model resulted in a good compromise between measurement accuracy and computational burden.
3. The good calibration of the model in the numerical environment correctly identifies the presence of damage in the vault, in good agreement with an experimental test.
4. The modal analysis, performed on the numerical model, showed about 10 percent reduction in the natural frequency of the first mode of the damaged structure compared to the intact structure. The frequency decay is less evident in the higher modes, but is still relevant, with an oscillation between 6 and 9 percent.

The observed frequency decay is a relevant aspect because it indicates a significant reduction in the stiffness of the vault due to the fire. This reduction in stiffness may have important implications for the structural safety of the vault, affecting its load-carrying capacity and its resistance to further applied loads.

This frequency decay observed in the numerical model can be used to assess the structural safety by applying a set of accelerometers to a physical structure and measuring frequencies based on the environmental vibrations. If a reasonably accurate numerical model is built, the frequency decays observed in the numerical simulation in correspondence with major damage to the structure can be compared with actual frequency measurements to assess the degree of damage to the physical structure after a fire; i.e., the numerical model is used as a digital twin of the physical structure.

The use of numerical models makes it possible to predict the state of degradation reached in the event of destructive events such as fires and to optimize the choice of the number of sensors to be used and their positioning with the aim of increasing the safety of technicians working in hazardous conditions.

Future developments of this study are related to the investigation of other case studies of masonry vaults to define a general trend in the frequency decay in ex ante and ex post fire conditions. Furthermore, a sensitivity analysis to identify the parameters which most affect the modal analysis is needed. Thus, if sufficiently accurate ex ante measurements of these parameters, so identified, can be ensured, a proper level of accuracy for the digital twin of the structure can be guaranteed. This approach could lead to defining a general procedure and rules for the investigation of historical structures made of masonry affected by fire phenomena.

Author Contributions: Conceptualization, A.L.S. and M.L.S.; methodology, A.L.S.; software, A.L.S. and P.L.; validation, A.L.S. and P.L.; formal analysis, A.L.S.; investigation, A.L.S., P.L., and D.F.; resources, A.L.S.; data curation, A.L.S.; writing—original draft preparation, A.L.S.; writing—review and editing, A.L.S., S.I. and M.L.S.; visualization, A.L.S. and S.I.; supervision, A.L.S., S.I. and D.F. All authors have read and agreed to the published version of the manuscript.

Funding: This research received no external funding.

Institutional Review Board Statement: Not applicable.

Informed Consent Statement: Not applicable.

Data Availability Statement: The original contributions presented in the study are included in the article, further inquiries can be directed to the corresponding authors.

Acknowledgments: We thank the Dipartimento dei Vigili del Fuoco, del soccorso pubblico e della difesa civile-Direzione Centrale per la prevenzione e la sicurezza tecnica-Area protezione passiva for the valuable support for the test conducted at Roma-Capannelle Laboratory and Ordine degli Ingegneri of Rome and Antonio Panaro, Francesco Tucci, Franco Viggiani, and Alberto Mazza for their helpful adivice and discussions.

Conflicts of Interest: The authors declare no conflicts of interest.

References

1. ISTAT Censimento Generale Della Popolazione e Delle Abitazioni. Available online: http://dati-censimentopopolazione.istat.it/Index.aspx?DataSetCode=DICA_EDIFICI1# (accessed on 28 February 2024).
2. *Annuario Statistico Del Corpo Nazionale Dei Vigili Del Fuoco*; 2023.
3. *Legge 30 Dicembre 2018, n. 145-Bilancio Di Previsione Dello Stato per l'anno Finanziario 2019 e Bilancio Pluriennale per Il Triennio 2019-2021. (18G00172)*; Italy, 2018.
4. *Decreto Ministeriale 14 Ottobre 2021-Approvazione Di Norme Tecniche Di Prevenzione Incendi per Gli Edifici Sottoposti a Tutela Ai Sensi Del Decreto Legislativo 22 Gennaio 2004, n. 42, Aperti al Pubblico, Contenenti Una o Più Attività Ricomprese Nell'all*; Ministero dell'Interno: Rome, Italy, 2021.
5. *Decreto Legislativo 22 Gennaio 2004, n. 42-Codice Dei Beni Culturali e Del Paesaggio, Ai Sensi Dell'articolo 10 Della Legge 6 Luglio 2002, n. 137*; Italy, 2004.
6. De Matteis, G.; Cacace, D.; Rouhi, J. Masonry Vaults: Architectural Evolution, Structural Behaviour and Collapse Mechanisms. In Proceedings of the 7th Structural Engineers World Congress 2019, İstanbul, Turkey, 24–26 April 2019.

7. Angjeliu, G.; Cardani, G.; Coronelli, D. Digital Modelling and Analysis of Masonry Vaults. *ISPRS Ann. Photogramm. Remote Sens. Spat. Inf. Sci.* **2019**, *42*, 83–89.
8. Creazza, G.; Matteazzi, R.; Saetta, A.; Vitaliani, R. Analyses of Masonry Vaults: A Macro Approach Based on Three-Dimensional Damage Model. *J. Struct. Eng.* **2002**, *128*, 646–654. https://doi.org/10.1061/ASCE0733-94452002128:5646.
9. Block, P.; Ochsendorf, J. Thrust Network Analysis: A New Methodology for Three-Dimensional Equilibrium. *J. Int. Assoc. Shell Spat. Struct.* **2007**, *48*, 167–173.
10. Milani, E.; Milani, G.; Tralli, A. Limit Analysis of Masonry Vaults by Means of Curved Shell Finite Elements and Homogenization. *Int. J. Solids Struct.* **2008**, *45*, 5258–5288. https://doi.org/10.1016/j.ijsolstr.2008.05.019.
11. Foraboschi, P. Strengthening of Masonry Arches with Fiber-Reinforced Polymer Strips. *J. Compos. Constr.* **2004**, *8*, 191–202. https://doi.org/10.1061/(ASCE)1090-0268(2004)8:3(191).
12. Heyman, J. The Stone Skeleton. *Int. J. Solids Struct.* **1966**, *2*, 249–256. https://doi.org/10.1016/0020-7683(66)90018-7.
13. O'Dwyer, D. Funicular Analysis of Masonry Vaults. *Comput. Struct.* **1999**, *73*, 187–197. https://doi.org/10.1016/S0045-7949(98)00279-X.
14. Heyman, J. The Stone Skeleton: Structural Engineering of Masonry Architecture. *Int. J. Rock Mech. Min. Sci. Geomech. Abstr.* **1996**, *3*, 133A.
15. Fantilli, A.P.; Burello, N.S. Masonry Arches and Vaults under Fire. *J. Build. Eng.* **2022**, *56*, 104740. https://doi.org/10.1016/j.jobe.2022.104740.
16. Parent, T.; Brocato, M.; Colas, A.S.; Domede, N.; Dubois, F.; Garnier, D.; Gros, A.; Mindeguia, J.C.; Morel, S.; Morenon, P.; et al. A Multi-Model Structural Analysis of the Vaults of Notre-Dame de Paris Cathedral after the 2019 Fire and a Proposal for a Hybrid Model Merging Continuum and Discrete Approaches. *J. Cult. Herit.* **2024**, *65*, 135–144. https://doi.org/10.1016/J.CULHER.2023.05.009.
17. Pellegrini, D. Thermo-Mechanical Analyses of Masonry Structures in Fire Conditions. *Finite Elem. Anal. Des.* **2024**, *234*, 104128. https://doi.org/10.1016/J.FINEL.2024.104128.
18. Luccioni, B.M.; Figueroa, M.I.; Danesi, R.F. Thermo-Mechanic Model for Concrete Exposed to Elevated Temperatures. *Eng. Struct.* **2003**, *25*, 729–742. https://doi.org/10.1016/S0141-0296(02)00209-2.
19. Rezende, C.; Simões, Y. de S.; Rodovalho, F. da S.; Nalon, G.H.; Santos, C.F.R.; Simões, Y. de S.; Rodovalho, F. da S.; Nalon, G.H. Thermo-Structural Modeling of Clay Units Masonry Walls under Fire Conditions. In Proceedings of XXXVIII Iberian Latin American Congress on Computational Methods in Engineering, Florianópolis, Brazil, 5–8 November 2017; ABMEC Brazilian Association of Computational Methods in Engineering.
20. Torregrosa, M.E.M.; Diez, J.C. Heat Transfer Mechanism and Thermomechanical Analysis of Masonry Structures (Mortars and Bricks) Subjected to High Temperatures. *Reactions and Mechanisms in Thermal Analysis of Advanced Materials*; John Wiley & Sons: Hoboken, NJ, USA, 2015; pp. 437–466.
21. Roca, P.; Cervera, M.; Gariup, G.; Pela', L. Structural Analysis of Masonry Historical Constructions. Classical and Advanced Approaches. *Arch. Comput. Methods Eng.* **2010**, *17*, 299–325. https://doi.org/10.1007/s11831-010-9046-1.
22. Ghiassi, B.; Oliveira, D.V.; Lourenço, P.B.; Marcari, G. Numerical Study of the Role of Mortar Joints in the Bond Behavior of FRP-Strengthened Masonry. *Compos. B Eng.* **2013**, *46*, 21–30. https://doi.org/10.1016/J.COMPOSITESB.2012.10.017.
23. Zucchini, A.; Lourenço, P.B. A Coupled Homogenisation–Damage Model for Masonry Cracking. *Comput. Struct.* **2004**, *82*, 917–929. https://doi.org/10.1016/J.COMPSTRUC.2004.02.020.
24. Senthivel, R.; Lourenço, P.B. Finite Element Modelling of Deformation Characteristics of Historical Stone Masonry Shear Walls. *Eng. Struct.* **2009**, *31*, 1930–1943. https://doi.org/10.1016/J.ENGSTRUCT.2009.02.046.
25. Lourenço, P.B. Computations on Historic Masonry Structures. *Prog. Struct. Eng. Mater.* **2002**, *4*, 301–319. https://doi.org/10.1002/pse.120.
26. Petracca, M.; Pelà, L.; Rossi, R.; Zaghi, S.; Camata, G.; Spacone, E. Micro-Scale Continuous and Discrete Numerical Models for Nonlinear Analysis of Masonry Shear Walls. *Constr. Build. Mater.* **2017**, *149*, 296–314. https://doi.org/10.1016/J.CONBUILDMAT.2017.05.130.
27. Sarhosis, V.; Lemos, J.V. A Detailed Micro-Modelling Approach for the Structural Analysis of Masonry Assemblages. *Comput. Struct.* **2018**, *206*, 66–81. https://doi.org/10.1016/J.COMPSTRUC.2018.06.003.
28. D'Altri, A.M.; de Miranda, S.; Castellazzi, G.; Sarhosis, V. A 3D Detailed Micro-Model for the in-Plane and out-of-Plane Numerical Analysis of Masonry Panels. *Comput. Struct.* **2018**, *206*, 18–30. https://doi.org/10.1016/J.COMPSTRUC.2018.06.007.
29. Diamanti, N.; Giannopoulos, A.; Forde, M.C. Numerical Modelling and Experimental Verification of GPR to Investigate Ring Separation in Brick Masonry Arch Bridges. *NDT E Int.* **2008**, *41*, 354–363. https://doi.org/10.1016/J.NDTEINT.2008.01.006.
30. Bolhassani, M.; Hamid, A.A.; Lau, A.C.W.; Moon, F. Simplified Micro Modeling of Partially Grouted Masonry Assemblages. *Constr. Build. Mater.* **2015**, *83*, 159–173. https://doi.org/10.1016/J.CONBUILDMAT.2015.03.021.
31. Grande, E.; Milani, G.; Sacco, E. Modelling and Analysis of FRP-Strengthened Masonry Panels. *Eng. Struct.* **2008**, *30*, 1842–1860. https://doi.org/10.1016/J.ENGSTRUCT.2007.12.007.
32. Grosman, S.; Bilbao, A.B.; Macorini, L.; Izzuddin, B.A. Numerical Modelling of Three-Dimensional Masonry Arch Bridge Structures. *Proc. Inst. Civ. Eng.-Eng. Comput. Mech.* **2021**, *174*, 96–113. https://doi.org/10.1680/jencm.20.00028.
33. Minga, E.; Macorini, L.; Izzuddin, B.A.; Caliò, I. 3D Macroelement Approach for Nonlinear FE Analysis of URM Components Subjected to In-Plane and out-of-Plane Cyclic Loading. *Eng. Struct.* **2020**, *220*, 110951. https://doi.org/10.1016/J.ENGSTRUCT.2020.110951.

34. Prakash, P.R.; Azenha, M.; Pereira, J.M.; Lourenço, P.B. Finite Element Based Micro Modelling of Masonry Walls Subjected to Fire Exposure: Framework Validation and Structural Implications. *Eng. Struct.* **2020**, *213*, 110545. https://doi.org/10.1016/j.engstruct.2020.110545.
35. Aras, F.; Krstevska, L.; Altay, G.; Tashkov, L. Experimental and Numerical Modal Analyses of a Historical Masonry Palace. *Constr. Build. Mater.* **2011**, *25*, 81–91. https://doi.org/10.1016/J.CONBUILDMAT.2010.06.054.
36. Ramos, L.F.; Marques, L.; Lourenço, P.B.; De Roeck, G.; Campos-Costa, A.; Roque, J. Monitoring Historical Masonry Structures with Operational Modal Analysis: Two Case Studies. *Mech. Syst. Signal Process.* **2010**, *24*, 1291–1305. https://doi.org/10.1016/J.YMSSP.2010.01.011.
37. Gentile, C.; Saisi, A. Operational Modal Testing of Historic Structures at Different Levels of Excitation. *Constr. Build. Mater.* **2013**, *48*, 1273–1285. https://doi.org/10.1016/j.conbuildmat.2013.01.013.
38. Döhler, M.; Lam, X.B.; Mevel, L. Uncertainty Quantification for Modal Parameters from Stochastic Subspace Identification on Multi-Setup Measurements. *Mech. Syst. Signal Process.* **2013**, *36*, 562–581. https://doi.org/10.1016/j.ymssp.2012.11.011.
39. Smith, M. *ABAQUS/Standard User's Manual, Version 6.12*; Dassault Systèmes Simulia Corp, Providence, USA.: 2009.
40. Milani, G.; Cattari, S.; Degli Abbati, S.; Ottonelli, S.; Magenes, G.; Manzini, C.F.; Morandi, P.; Camata, G.; Spacone, E.; Marano, C.; et al. *Uso Dei Software Di Calcolo Nella Verifica Sismica Degli Edifici in Muratura*; **2020**.
41. Bićanić, N.; Stirling, C.; Pearce, C.J. Discontinuous Modelling of Masonry Bridges. *Comput. Mech.* **2003**, *31*, 60–68. https://doi.org/10.1007/s00466-002-0393-0.
42. Sacco, E.; Lebon, F. A Damage–Friction Interface Model Derived from Micromechanical Approach. *Int. J. Solids Struct.* **2012**, *49*, 3666–3680. https://doi.org/10.1016/J.IJSOLSTR.2012.07.028.
43. Serpieri, R.; Albarella, M.; Sacco, E. A 3D Microstructured Cohesive–Frictional Interface Model and Its Rational Calibration for the Analysis of Masonry Panels. *Int. J. Solids Struct.* **2017**, *122–123*, 110–127. https://doi.org/10.1016/J.IJSOLSTR.2017.06.006.
44. Lubliner, J.; Oliver, J.; Oller, S.; Oñate, E. A Plastic-Damage Model for Concrete. *Int. J. Solids Struct.* **1989**, *25*, 299–326. https://doi.org/10.1016/0020-7683(89)90050-4.
45. Hillerborg, A.; Modéer, M.; Petersson, P.-E. Analysis of Crack Formation and Crack Growth in Concrete by Means of Fracture Mechanics and Finite Elements. *Cem. Concr. Res.* **1976**, *6*, 773–781. https://doi.org/10.1016/0008-8846(76)90007-7.
46. Lemaitre, J. Coupled Elasto-Plasticity and Damage Constitutive Equations. *Comput. Methods Appl. Mech. Eng.* **1985**, *51*, 31–49. https://doi.org/10.1016/0045-7825(85)90026-X.
47. Lee, J.; Fenves, G.L. Plastic-Damage Model for Cyclic Loading of Concrete Structures. *J. Eng. Mech.* **1998**, *124*, 892–900. https://doi.org/10.1061/(ASCE)0733-9399(1998)124:8(892).
48. *Prova Di Resistenza al Fuoco Su Una Volta a Botte in Muratura*; Vigili del Fuoco-Direzione Centrale per la Prevenzione e la Sicurezza Tecnica Area Protezione Passiva-Settore Resistenza al fuoco: Rome, Italy, 2007.
49. Ministero delle Infrastrutture e dei Trasporti Testo Aggiornato Delle Norme Tecniche per Le Costruzioni (NTC2018), Di Cui Alla Legge 5 Novembre 1971, n. 1086, Alla Legge 2 Febbraio 1974, n. 64, al Decreto Del Presidente Della Repubblica 6 Giugno 2001, n. 380, Ed al Decreto Legge 28 Maggio 2004, n. 136 2018. Available online: https://www.gazzettaufficiale.it/eli/id/2018/2/20/18A00716/sg (accessed on 28 February 2024).
50. Naciri, K.; Aalil, I.; Chaaba, A. Numerical Analysis of the Brick Shape and Bond Pattern Effects on the Masonry Cyclic Behavior: A New Brick Shape to Improve the Masonry Seismic Performance. *Asian J. Civ. Eng.* **2022**, *23*, 67–86.
51. Naciri, K.; Aalil, I.; Chaaba, A.; Al-Mukhtar, M. Numerical Modeling of a Masonry Arch Structure. *Procedia Struct. Integr.* **2022**, *37*, 469–476. https://doi.org/10.1016/J.PROSTR.2022.01.111.
52. Drucker, D.C.; Prager, W. Soil Mechanics and Plastic Analysis or Limit Design. *Q. Appl. Math.* **1952**, *10*, 157–165.
53. Drucker, D.C. Relation of Experiments to Mathematical Theories of Plasticity. *J. Appl. Mech.* **1949**, *16*, 349–357.
54. Dauda, J.; Iuorio, O.; Lourenco, P. Characterization of Brick Masonry: Study towards Retrofitting URM Walls with Timber-Panels. In Proceedings of the 10th International Masonry Conference (10thIMC), Milan, Italy, 9–11 July 2018.
55. Ptaszkowska, J.; Oliveira, D. Numerical Modeling of Masonry Vaults Strengthened with Transversal Diaphragms. Master Thesis, Universidade do Minho, Braga, Portugal, 2013.
56. Abdulla, K.F.; Cunningham, L.S.; Gillie, M. Simulating Masonry Wall Behaviour Using a Simplified Micro-Model Approach. *Eng. Struct.* **2017**, *151*, 349–365. https://doi.org/10.1016/J.ENGSTRUCT.2017.08.021.
57. *EN 1996-1-2:2005*; Eurocode 6-Design of Masonry Structures-Part 1–2: General Rules-Structural Fire Design. European Committee for Standardization (CEN), Brussels, Belgium, 2010. Available online: https://www.phd.eng.br/wp-content/uploads/2015/02/en.1996.1.2.2005.pdf (accessed on 28 February 2024)
58. Circolare Del Ministero Dell'Interno DCPREV n. 4638 Del 5/4/2015 "Pubblicazione in Gazzetta Ufficiale Degli Annessi Nazionali Degli Eurocodici". Available online: https://www.gazzettaufficiale.it/gazzetta/serie_generale/caricaDettaglio?dataPubblicazioneGazzetta=2013-03-27&numeroGazzetta=73 (accessed on 28 February 2024).
59. Decreto Ministeriale Del 14 Febbraio 2020: Aggiornamento Della Sezione V Dell'allegato 1 al Decreto 3 Agosto 2015, Concernente l'approvazione Di Norme Tecniche Di Prevenzione Incendi. (20A01155) (GU Serie Generale n.57 Del 06-03-2020) 2020. Available online: https://www.gazzettaufficiale.it/eli/id/2020/03/06/20A01155/sg (accessed on 28 February 2024).
60. *ISO 834-10:2014*; Fire Resistance Tests. International Organization for Standardization: Geneva, Switzerland, 2014.
61. Chopra, A.K. *Dynamics of Structures*; Prentice-Hall international series in civil engineering and engineering mechanics; Pearson Education: London, UK, 2007; ISBN 9788131713297.

62. Brincker, R.; Ventura, C. *Introduction to Operational Modal Analysis*; John Wiley and Sons Ltd.: Chichester, UK, 2015.
63. Rainieri, C.; Fabbrocino, G. *Operational Modal Analysis of Civil Engineering Structures: An Introduction and Guide for Applications*; Springer: New York, NY, USA, 2014; ISBN 978-1-4939-0767-0.
64. Fan, W.; Qiao, P. Vibration-Based Damage Identification Methods: A Review and Comparative Study. *Struct. Health Monit.* **2010**, *10*, 83–111. https://doi.org/10.1177/1475921710365419.
65. Alvandi, A.; Cremona, C. Assessment of Vibration-Based Damage Identification Techniques. *J. Sound Vib.* **2006**, *292*, 179–202. https://doi.org/10.1016/J.JSV.2005.07.036.
66. Gentile, C.; Saisi, A. Ambient Vibration Testing of Historic Masonry Towers for Structural Identification and Damage Assessment. *Constr. Build. Mater.* **2007**, *21*, 1311–1321. https://doi.org/10.1016/J.CONBUILDMAT.2006.01.007.
67. Magalhães, F.; Cunha, A.; Caetano, E. Vibration Based Structural Health Monitoring of an Arch Bridge: From Automated OMA to Damage Detection. *Mech. Syst. Signal Process.* **2012**, *28*, 212–228. https://doi.org/10.1016/J.YMSSP.2011.06.011.
68. Mansour, S.; Rizzo, F.; Giannoccaro, N.I.; La Scala, A.; Sabbà, M.F.; Foti, D. Essential Dynamic Characterization of a Historical Bridge: Integrated Experimental and Numerical Investigations. *J. Civ. Struct. Health Monit.* **2024**, *14*, 85–102. https://doi.org/10.1007/s13349-023-00744-y.
69. Foti, D.; Giannoccaro, N.I.; Sabbà, M.F.; La Scala, A. Dynamic Identification of a Strategic Building of the Sixties with a Mixed Structure. *Procedia Struct. Integr.* **2023**, *44*, 782–789. https://doi.org/10.1016/J.PROSTR.2023.01.102.
70. Diaferio, M.; Foti, D.; La Scala, A.; Sabbà, M.F. Selection Criteria of Experimental Setup for Historical Structures. In Proceedings of the 2021 AEIT International Annual Conference (AEIT), Milan, Italy, 4–8 October 2021; pp. 1–6.